Nanoscale

PAPER

View Article Online
View Journal | View Issue



Cite this: *Nanoscale*, 2022, **14**, 17230

# *In situ* interfacial passivation with an arylphosphine oxide and phosphonate electron transporting layer for efficient all-solution-processed PeQLEDs†

Xuefei Li,[a,c] Yiting Tian,[b] Liuqing Yang,[a,c] Shumeng Wang, *[c] Lei Zhao*[c] and Junqiao Ding *[a,c]

Perovskite quantum dot light-emitting diodes (PeQLEDs) have emerged as a promising candidate for high-quality lightings and displays, where an electron transporting layer (ETL) is required to achieve balanced charge transport and thus high performance. However, the ETL is often thermally-deposited under vacuum, since the low-cost solution process would damage the underlying perovskite quantum dots (PeQDs). Here, we demonstrate efficient all-solution-processed PeQLEDs based on arylphosphine oxide (SPPO13) and phosphonate (TPPO) as the ETL. Benefitting from the coordination between P═O and exposed Pb atoms, *in situ* interfacial passivation occurs during the solution deposition of SPPO13 or TPPO on PeQDs. As a result, bilayer films (PeQDs/ETL) exhibit improved photoluminescence quantum yields and prolonged lifetimes compared with single layer PeQDs. Correspondingly, all-solution-processed PeQLEDs are fabricated successfully *via* an orthogonal solvent strategy, revealing bright green emission with a promising current efficiency of 24.1 cd $A^{-1}$ (12.1 lm $W^{-1}$, 6.47%) and CIE coordinates of (0.12, 0.79).

Received 11th July 2022,
Accepted 23rd October 2022

DOI: 10.1039/d2nr03793a

rsc.li/nanoscale



## Introduction

Perovskite quantum dots (PeQDs), as a candidate for next-generation lightings and displays,[1–3] have attracted intense attention due to their low-cost solution processability and excellent optical properties, such as high photoluminescence quantum yields (PLQYs), narrowband emissions and tunable wavelengths.[4–7] Since the first report of perovskite quantum dot light-emitting diodes (PeQLEDs) in 2015,[8] the efficiency has achieved a rapid rise.[9–15] Despite this, they still rely on the high-cost vacuum-deposited electron transporting layer (ETL) to obtain excellent device performance, which is not suitable for large-area and low-cost manufacturing in industrial mass production. The all-solution-processed PeQLEDs are a good pathway to solve this issue, because they could be fabricated through large-area and low-cost printing methods (inkjet or roll-to-roll printing). However, the solution construction of the PeQDs/ETL multilayer structure still remains a big challenge, since the deposition solvent of the ETL could redissolve the underlying PeQD layer.

To address such a problem, two main strategies have been developed including cross-linkable PeQD layer and orthogonal solvent processing. In the case of the former, the PeQD light-emitting layer is cross-linked to achieve excellent resistance to the processing solvent of the ETL. For example, Li *et al.* developed a trimethylaluminum vapor-based cross-linking method with an atomic layer deposition system to fix the PeQD film in place.[16] Wei *et al.* demonstrated an *in situ* light-initiated ligand cross-linking method to create a cross-linked PeQD film by incorporating conjugated linoleic acid as the ligand of PeQDs.[17] On the other hand, a simple orthogonal solvent processing strategy is applicable, where the PeQDs and ETL are produced in an alternative sequence of non-polar and polar solvents. As a result of the ionic nature of perovskite and the nonpolar property of surface ligands,[18] PeQDs are very easy to be redissolved or destroyed during the solution process. So a clever choice of ETL deposition solvents is required, such as esters, hydrofluoroethers[19] and chlorobenzene. For instance, Li *et al.* developed all-solution-processed PeQLEDs by using methyl acetate as the ETL solvent.[20] The resultant devices

[a]*School of Chemical Science and Technology, Yunnan University, Kunming 650091, P. R. China. E-mail: dingjunqiao@ynu.edu.cn*
[b]*School of Materials and Energy, Yunnan University, Kunming 650091, P. R. China*
[c]*State Key Laboratory of Polymer Physics and Chemistry, Changchun Institute of Applied Chemistry, Chinese Academy of Sciences, Changchun, 130022, P. R. China. E-mail: wangshumeng@ciac.ac.cn, zhaol@ciac.ac.cn*

†Electronic supplementary information (ESI) available: Properties of the PeQDs of $Cs_{0.70}FA_{0.30}PbBr_3$, solvent resistance of the PeQD film, XPS and FTIR spectra, device structure and characteristics, and performance comparison of all-solution-processed PeQLEDs. See DOI: https://doi.org/10.1039/d2nr03793a

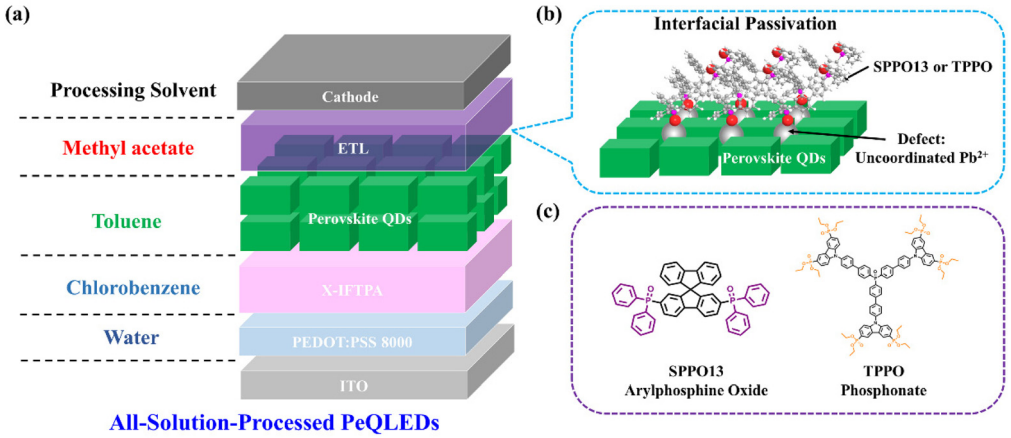


**Fig. 1** All-solution-processed PeQLEDs based on SPPO13 and TPPO as the ETL: (a) device configuration and processing method for each layer; (b) schematic diagram of *in situ* passivation at the interface between the PeQDs and the ETL; (c) molecular structures of the used ETLs.

exhibit a bright luminance with a maximum current efficiency of 3.26 cd $A^{-1}$. Despite the success, we note that the used polar solvent may induce additional defects on the surface of the PeQD film. From this point of view, it is highly desirable to passivate the emerging defects at the interface between PeQDs and the ETL during the solution deposition of the ETL.

With this idea in mind, we demonstrate efficient all-solution-processed PeQLEDs based on arylphosphine oxide-contained SPPO13 and phosphonate-contained TPPO as the ETL. As depicted in Fig. 1, both SPPO13 and TPPO are readily soluble in the polar solvent of methyl acetate, ensuring the successful fabrication of multilayer PeQLEDs *via* orthogonal solvent processing. Most importantly, the involved P═O group can coordinate with the exposed Pb atoms, leading to *in situ* passivation for the generated defects at the interface between PeQDs and the ETL. As a result, the PLQY of the bilayer PeQDs/ETL was found to be improved significantly (47.1–70.5%) compared with the single PeQD layer (22.7% and 33.4% for films with and without methyl acetate spin-rinsing). The corresponding devices are optimized to give a record-high current efficiency of 24.1 cd $A^{-1}$ (12.1 lm $W^{-1}$, 6.47%), which is among the highest ever reported for all-solution-processed PeQLEDs.

## Results and discussion

### Solvent resistance of the PeQD film

Green-emitting $Cs_{0.70}FA_{0.30}PbBr_3$ PeQDs were synthesized through a room temperature method as previously reported,[21,22] and then redispersed in anhydrous toluene prior to use (Fig. S1†). First, the solvent resistance of the PeQD film was investigated in order to choose a suitable processing solvent for the upper ETL (Table S1†). UV-Vis absorption spectra were recorded to monitor the thickness variation before and after spin-rinsing with different solvents (Fig. S2†). Except for chlorobenzene and methanol, the PeQD film could well resist most of the solvents with a remaining thickness of above 90% after spin-rinsing (Fig. 2a). Second, the dependence of the PL intensity on different solvents was further exploited

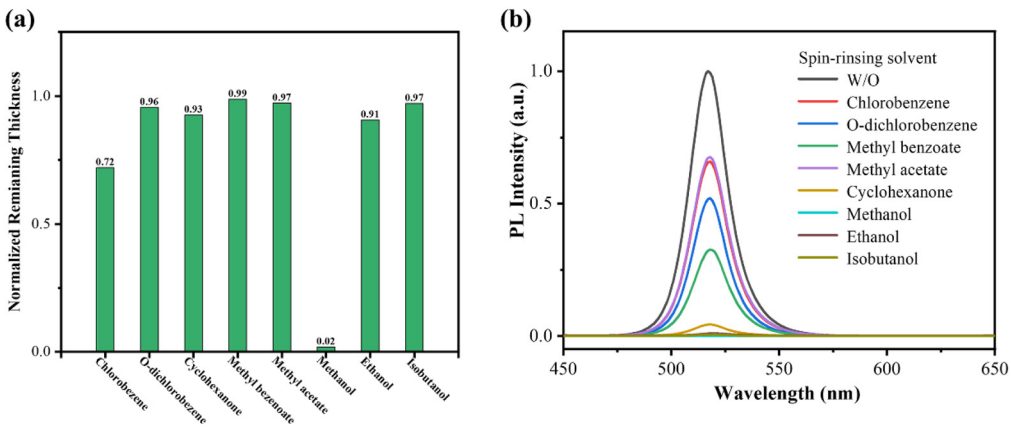


**Fig. 2** Solvent resistance of the PeQD film: (a) the remaining thickness after spin-rinsing with different solvents; (b) comparison of the PL intensity with and without spin-ringing.

to illustrate the quenching effect of the luminescent PeQD film (Fig. 2b). As for chlorobenzene and methanol, the decrease of PL intensity could be mainly ascribed to the fact that they both ruin the PeQD film with a remaining thickness of 72% and 2%, respectively. The strong polar solvents including cyclohexanone, ethanol and isobutanol are able to disintegrate the perovskite ionic crystal structures, and completely quench the PeQD luminance. This is further verified by the discontinuous and particle-agglomerating morphology observed in their atomic force microscopy (AFM) images (Fig. S3†). By contrast, weak polar solvents including *o*-chlorobenzene, methyl benzoate and methyl acetate are found to partly reduce the luminance of the PeQD film and cause slight agglomeration with increased surface. These phenomena could be explained by that PeQDs on the surface were re-dispersed in weak polar solvents because of their amphiphilic nature and then re-aggregated to form large aggregations. In this process, the unwanted defects newly appear and result in decreased luminescence properties. Given the large remaining thickness of 97% and the highest PL intensity after spin-rinsing, methyl acetate was finally selected as the processing solvent of the upper ETL.

### *In situ* interfacial passivation

In the case of all-solution-processed PeQLEDs, some defects inevitably occur on the underlying PeQD layer during the deposition of the ETL from its polar solution. To compensate for the luminance loss, the formed defects are better passivated *in situ* at the interface between the PeQDs and the ETL. That is, the upper ETL is required to have good defect passivation capability in itself. Therefore, SPPO13 containing arylphosphine oxide and TPPO containing phosphonate areselected as the ETL, because the lone pair electrons of P═O could act as a lewis base to coordinate with the redundant lead ions on the PeQD surface. Moreover, the polar nature of P═O makes SPPO13 and TPPO soluble in methyl acetate, ensuring the successful fabrication of multi-layer PeQLEDs *via* orthogonal solvent processing.

To demonstrate their *in situ* interfacial passivation, the photophysical characteristics of the bilayer films (PeQDs/SPPO13 and PeQDs/TPPO) are explored in comparison to the single layer (PeQDs) with and without methyl acetate spin-rinsing. As one can see in Fig. 3, the methyl acetate spin-rinsing is found to decrease the PL intensity with a decrease in PLQY from 33.3% to 22.7% due to the generation of new defects. Fortunately, when a solution of SPPO13 or TPPO in methyl acetate is spin-coated onto PeQDs, the bilayer film shows a distinct luminance enhancement under a UV lamp, accompanied by significantly improved PLQYs of 70.5% and 47.1%, respectively. Furthermore, transient photoluminance (PL) spectra, detected at the PeQD emission peak of 517 nm, were also performed to investigate the change in the exciton decay process. Compared with the initial one, the average PL decay lifetime is down from 5.64 ns to 2.55 ns for the spin-rinsed PeQD film, indicative of defect induced non-radiation. Nevertheless, the lifetime is obviously increased to 8.76 ns and 7.16 ns, respectively, when spin-coated by SPPO13 and TPPO in their methyl acetate solutions. In good agreement with the PL variation, the lifetime difference means that the interfacial defects between the PeQDs and the ETL can be passivated by SPPO13 and TPPO *in situ*, thus leading to suppressed non-radiation.

X-ray photoelectron spectroscopy (XPS) and Fourier transform infrared (FTIR) spectra were further recorded to verify the interaction between PeQDs and SPPO13 or TPPO (Fig. 4).

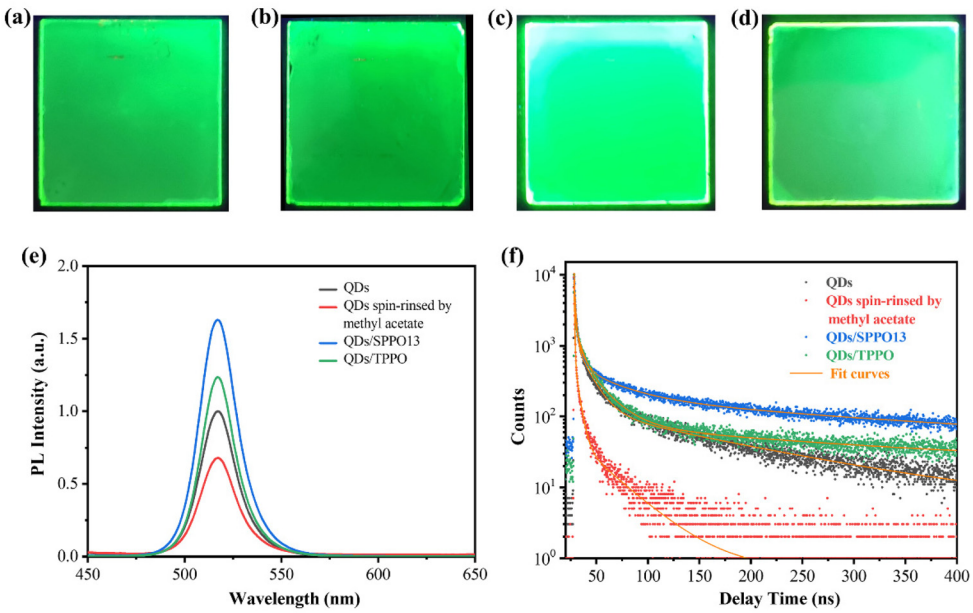


Fig. 3 *In situ* interfacial passivation: (a–d) photographs under the UV lamp for the pristine PeQD film, the PeQD film spin-rinsed with methyl acetate, and the PeQD films coated with SPPO13 and TPPO from left to right; (e) steady-state PL spectra; (f) transient PL spectra.

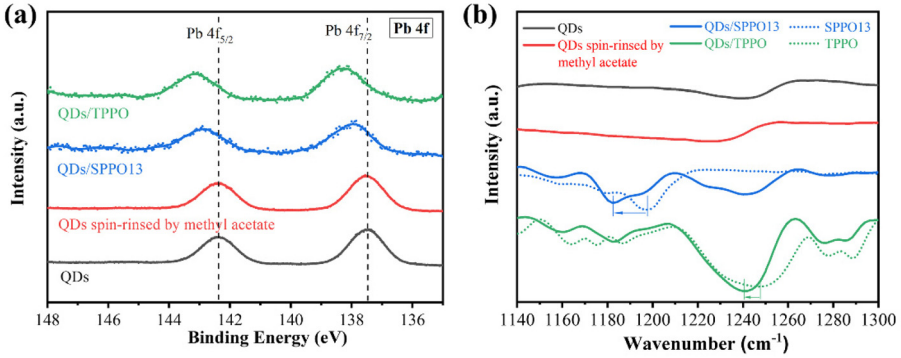


**Fig. 4** Coordination between P═O and exposed Pb atoms: (a) Pb 4f core XPS spectra; (b) magnified FTIR spectra ranged from 1140 to 1300 $cm^{-1}$.

Compared with the initial and spin-rinsed PeQDs, the Pb 4f peaks of the PeQDs/SPPO13 and PeQDs/TPPO films shift towards a higher binding energy (BE). At the same time, their P 2p peaks also move towards a higher BE with respect to pure SPPO13 and TPPO films (Fig. S4†). The observed similar trend confirms the coordination between the P═O group and the Pb atom. In the FTIR spectra of the SPPO13 or TPPO modified films, the characteristic peaks at 1197 $cm^{-1}$ for SPPO13 and 1247 $cm^{-1}$ for TPPO newly appear and are found to be down-shifted slightly, an indicator of the interaction between PeQDs and SPPO13 or TPPO. As mentioned above, the solution deposition of the ETL onto the PeQD layer is anticipated to cause exposed Pb atoms as the main defects because of the desorption of surface ligands to some degree. Meanwhile, benefitting from the coordination between P═O and Pb, the generated defects at the interface between the PeQDs and the ETL can be effectively passivated *in situ* so as to recover or even improve the photophysical properties of PeQDs (Table 1).

### All-solution-processed PeQLEDs

In view of *in situ* passivation, SPPO13 may act as a potential ETL for all-solution-processed PeQLEDs. To evaluate this, multilayer devices were assembled with a configuration of ITO/PEDOT:PSS (40 nm)/X-IFTPA (20 nm)/PeQDs (40 nm)/ETL (40 nm)/Al (100 nm) (Fig. 1 and S6†). Here the hole injection layer of PEDOT:PSS, the cross-linkable hole transporting layer of X-IFTPA, the emitting layer of PeQDs and the ETL of SPPO13 were solution-deposited in sequence from water, chlorobenzene, toluene and methyl acetate, respectively. As plotted in Fig. 5a, the electroluminescence (EL) spectra show strong green emission from PeQDs, which peaked at 520 nm together with a full width at half maximum (FWHM) of 19 nm and Commission Internationale de l'Eclairage (CIE) coordinates of (0.12, 0.79). An acceptable current efficiency of 9.02 cd $A^{-1}$ (4.69 lm $W^{-1}$, 2.41%) and a maximum luminance of 7201.7 cd $m^{-2}$ are achieved when SPPO13 is used as the ETL (Fig. S7† and Table 2).

Although the solution-processed SPPO13 layer works well to transport electrons, there still exists a large electron injection barrier induced by the unmatched lowest unoccupied molecular orbital (LUMO) energy level of SPPO13 (−2.65 eV) relative to the work function of the Al cathode (4.28 eV). To solve this problem, two routes are tried: one is to adopt a mixed ETL of SPPO13 : TPPO by incorporating TPPO with good electron injection capability into SPPO13, and the other is to introduce an extra Liq electron injection layer on SPPO13. As a result of improved electron injection, the turn-on voltage is reduced from 4.4 V to 4.2 V and 4.0 V for SPPO13 : TPPO and SPPO13/Liq devices, respectively, whereas the CIE coordinates remain almost unchanged. Correspondingly, the maximum current efficiency is optimized to be 13.6 cd $A^{-1}$ (6.88 lm $W^{-1}$, 3.63%) and 24.1 cd $A^{-1}$ (12.1 lm $W^{-1}$, 6.47%), and the luminance goes up to 12 125.6 cd $m^{-2}$ and 12 058.6 cd $m^{-2}$ (Fig. 5b and S7†). To our knowledge, the obtained performance is the best ever reported for all-solution-processed PeQLEDs (Fig. S8 and Table S2†).[16,17,19,20,23–26] The optimized device exhibits a limited operating lifetime (Fig. S9†), which could be ascribed to the ubiquitous ionic migration under an electric field for perovskite materials.

To investigate the electron injection behavior, electron-only devices (EODs) are prepared and the current density–voltage (*J*–*V*) curves are shown in Fig. 5c. Following a sequence of SPPO13, SPPO13 : TPPO and SPPO13/Liq, it is found that the

**Table 1** The summary of the photophysical parameters of the PeQD film

| Film[a] | $\lambda_{em}$ (nm) | PLQY (%) | $\tau_{ave}$ [b] (ns) | $K_r$ [c] ($10^{-2}$ $ns^{-1}$) | $K_{nr}$ [c] ($10^{-2}$ $ns^{-1}$) |
|---|---|---|---|---|---|
| QDs | 517 | 33.4 | 5.64 | 5.92 | 11.8 |
| QDs spin-rinsed by methyl acetate | 517 | 22.7 | 2.55 | 8.90 | 30.3 |
| QDs/SPPO13 | 517 | 70.5 | 8.76 | 8.05 | 3.37 |
| QDs/TPPO | 517 | 47.1 | 7.16 | 6.58 | 7.38 |

[a] Measured by using an integrating sphere and excited at 400 nm. [b] The lifetimes were determined by the triple exponential fit of PL decay curves. [c] $\tau_{ave}$, $k_r$ and $k_{nr}$ were calculated based on the following formulas: $\tau_{ave} = \frac{\sum_{i=1}^{3} a_i\tau_i^2}{\sum_{i=1}^{3} a_i\tau_i} = \frac{1}{k_r + k_{nr}}$, $k_r = \frac{PLQY}{\tau_{ave}}$, and $k_{nr} = \frac{1}{\tau_{ave}} - k_r$ ($a_i$ and $\tau_i$ are the normalized coefficients and time constants, respectively).

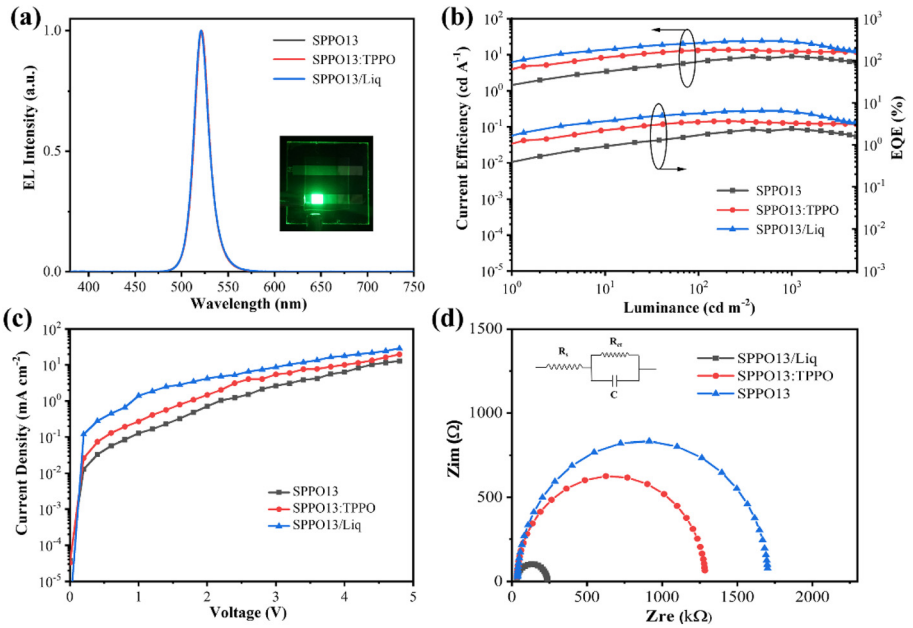


**Fig. 5** Device performance with varied ETLs: (a) EL spectra at 100 cd m$^{-2}$ (inset: photograph of the working device based on SPPO13/Liq); (b) current efficiency and external quantum efficiency (EQE) as a function of luminance; (c) current–voltage curves for electron-only devices; (d) impedance spectra (inset: the equivalent circuit model).

**Table 2** Summary of the device performance of the PeQLEDs

| ETL | $V_{on}$ [a] (V) | $L$ [b] (cd m$^{-2}$) | CE [b] (cd A$^{-1}$) | PE [b] (lm W$^{-1}$) | EQE [b] (%) | CIE ($x$, $y$) |
|---|---|---|---|---|---|---|
| SPPO13 | 4.4 | 7201.65 | 9.02 | 4.69 | 2.41 | (0.12, 0.79) |
| SPPO13 : TPPO | 4.2 | 12 125.6 | 13.6 | 6.88 | 3.63 | (0.12, 0.79) |
| SPPO13/Liq | 4.0 | 12 058.6 | 24.1 | 12.1 | 6.47 | (0.12, 0.79) |

[a] Turn-on voltage at 1 cd m$^{-2}$. [b] Maximum data. $L$: luminance; CE: current efficiency; PE: power efficiency; EQE: external quantum efficiency; and CIE: Commission Internationale de l'Eclairage.

electron current is gradually increased, indicating the improved electron injection. Meanwhile, impedance spectroscopy is also measured to study the carrier transport balance (Fig. 5d), and a simple resistance-capacitance (RC) circuit is used to model the EL process in PeQLEDs. The recombination resistance was calculated to be 1.67, 1.25 and 0.21 kΩ for SPPO13, SPPO13 : TPPO and SPPO13/Liq devices, respectively. The tendency is understandable when considering the enhanced electron injection can balance the carrier transport and then suppress the excess hole accumulation in PeQLEDs. In other words, the more balanced carrier transport in the SPPO13/Liq device is within our expectation to enhance the hole–electron recombination possibility, which accounts for the much better device performance.

## Conclusions

In summary, high-performance all-solution-processed PeQLEDs have been demonstrated based on arylphosphine oxide-contained SPPO13 and phosphonate-contained TPPO as the ETL. The polar nature of P═O makes SPPO13 and TPPO readily soluble in methyl acetate, in which the PeQD film has perfect resistance. Through the coordination between the P═O group and exposed Pb atoms, most importantly, the defects generated by methyl acetate at the PeQDs/ETL interface could be effectively passivated *in situ* during the deposition of the ETL. Consequently, all-solution-processed PeQLEDs are assembled successfully, revealing a promising current efficiency of 24.1 cd A$^{-1}$ (12.1 lm W$^{-1}$, 6.47%) after optimization. The results highlight the great potential of orthogonal solvents in the fabrication of efficient all-solution-processed PeQLEDs.

## Experimental

### Materisls

Cesium carbonate ($Cs_2CO_3$, 99.9%), formamidine acetate (FA(Ac), 99%), lead bromide ($PbBr_2$, 99.999%), zinc bromide ($ZnBr_2$, 99.999%), didodecyldimethylammonium bromide (DDAB, 98%), octanoic acid (OTA, 99%) and tetraoctylammo-

 

nium bromide (TOAB, 98%), ethyl acetate (EtOAc, 99.8%), methyl acetate (MeOAc, 99.5%), methol (99.8%), ethanol (99.8%), isobutanol (99%), methyl benzoate (99%), cyclohexanone (99.8%) and *o*-dichlorobenzene (99%) were purchased from Sigma-Aldrich. Toluene and chlorobenzene were purchased from Beijing Chemical Plant. Poly(3,4-ethylenedioxythiophene)-poly(styrenesulfonate) (PEDOT:PSS, 8000) was purchased from Heraeus Precious Metals GmbH & Co. KG. 2,7-Bis (diphenylphosphoryl)-9,9′-spirobifluorene (SPPO13, 99%) and 8-hydroxyquinolinolato-lithium (Liq, 99.5%) were purchased from Luminescence Technology Corp. Except for toluene and chlorobenzene that were distilled before use, other materials and solvents were used as received. X-IFTPA and TPPO were synthesized in our laboratory according to the literature methods.[27,28]

### Synthesis of $Cs_{0.70}FA_{0.30}PbBr_3$ QDs

$Cs_{0.70}FA_{0.30}PbBr_3$ QDs were synthesized by the method previously reported.[21,22] Firstly, a cesium precursor was prepared by adding 0.2 mmol $Cs_2CO_3$ (0.0652 g) into 2 ml of OTA (0.1 mM) and a formamidine precursor was prepared by adding 0.2 mmol FA(Ac) (0.0208 g) into 1 ml of OTA (0.2 mM). The $PbBr_2$ precursor was prepared by adding 1 mmol $PbBr_2$ (0.3670 g) and 2 mmol TOAB (1.0936 g) into 10 ml of toluene (0.1 mM). The $ZnBr_2$ precursor was dissolved in 0.2 mmol $ZnBr_2$ (0.0450 g) and 0.4 mmol TOAB was dissolved in 2 ml of toluene. All the precursors were stirred at room-temperature until a clear and completely dissolved solution was formed. A mixture of 0.7 ml of Cs precursor and 0.3 ml of FA precursor was prepared before the synthesis of QDs. Then, 1 ml of Cs : FA mixture was swiftly added into 9 ml of $PbBr_2$ precursor solution. The reaction was stirred for 2 min at room-temperature. Subsequently, 3 ml of DDAB (in toluene with a concentration of 10 mg $ml^{-1}$) was added. After 3 min, 450 μl of the $ZnBr_2$–toluene solution was added to the QD solution for passivating the QDs. After stirring for 5 min, ethyl acetate was added to the crude solution with a volume ratio of 2 : 1, and then the precipitate was collected and dispersed in toluene after centrifugation at 10 000 rpm for 5 min. The same washing process with ethyl acetate was repeated twice again and the precipitate was collected and re-dispersed in toluene at a concentration of 30 mg $ml^{-1}$ for future use.

### Measurements and characterization

The UV-Vis absorption spectra of all $Cs_{0.70}FA_{0.30}PbBr_3$ QDs solution and films were recorded using a Perkin-Elmer Lambda 35 UV-Vis spectrometer. The thickness variation of QD films before and after spin-rinsing with solvents was calculated according to a change in the peak intensity at 300 nm for the UV-Vis absorption spectra. PL spectra and PLQYs were recorded using a HORIBA FL3C-111 spectrometer with an integrating sphere system. Transient PL spectra were recorded on an Edinburgh fluorescence spectrometer (FLS-980). Transmission electron microscopy (TEM) was carried out with an FEI Tecnai G2 F20. X-ray photoelectron spectroscopy (XPS) measurements were performed on a Thermo ESCALAB 250 photoelectron spectrometer. Fourier transform infrared (FTIR) spectroscopy was performed using a VERTEX 70 FTIR spectrometer. A Dimension Icon AFM tool was utilized to measure the morphologies of the PeQD films.

### Device preparation and characterization

All-solution-processed PeQLEDs based on the $Cs_{0.70}FA_{0.30}PbBr_3$ QDs were prepared with a structure of ITO/PEDOT:PSS (40 nm)/X-IFTPA (20 nm)/$Cs_{0.70}FA_{0.30}PbBr_3$ QDs (40 nm)/SPPO13 (or SPPO13 : TPPO, or SPPO13/Liq (1 nm)) (40 nm)/Al (100 nm). Dispersion of PEDOT:PSS in water was spin-coated onto cleaned and ultraviolet-ozone (UVO) treated ITO substrates. After being baked at 120 °C for 30 min in air, the hole transporting layer of X-IFTPA was spin-coated onto PEDOT:PSS from its chlorobenzene solution at a concentration of 4 mg $ml^{-1}$, and then annealed at 180 °C for 0.5 h. The PeQDs were spin-coated onto X-IFTPA at 1500 rpm for 60 s and annealed at 80 °C for 30 min in a glovebox. Subsequently, the electron transporting material of SPPO13 or mixed SPPO13 : TPPO (8 : 2) was spin-coated onto the emitting layer (EML) from its methyl acetate solution at a concentration of 3.5 mg $ml^{-1}$, and then annealed at 70 °C for 15 min under nitrogen to form an ETL. For the ETL of SPPO13/Liq, an extra interlayer of Liq (1 nm) was deposited using thermal evaporation. Finally, Al (100 nm) was deposited using thermal evaporation at a pressure under $4 \times 10^{-4}$ Pa. The active area of the device was 14 $mm^2$. The electron-only devices with a structure of Al/$Cs_{0.70}FA_{0.30}PbBr_3$ QDs (40 nm)/SPPO13 (or SPPO13 : TPPO, or SPPO13/Liq (1 nm)) (40 nm)/Al (100 nm) were prepared following the same process as that mentioned above. The current density–voltage–luminance (*J*–*V*–*L*) characteristics were measured using a Keithley source measurement unit (calibrated silicon photodiode, Keithley 2400 and Keithley 2000), and the EL spectra were recorded using a CS2000A spectrometer. All the measurements were carried out at room temperature in air. The EQE was calculated from the luminance, current density and EL spectra assuming a Lambertian distribution. Impedance spectroscopy measurements were carried out using a PARSTAT 3000A potentiostat in the 1 MHz–1 Hz frequency range with an applied voltage of 6.0 V and an AC signal of 100 mV.

## Conflicts of interest

There are no conflicts to declare.

## Acknowledgements

The authors acknowledge the financial support from the National Natural Science Foundation of China (no. 51873205 and 52173186), the Scientific Research Foundation for Introduced Talents of Yunnan University (CZ21623201), and the Youth Innovation Promotion Association, CAS (2021222).

## References

1 M. V. Kovalenko, L. Protesescu and M. I. Bodnarchuk, *Science*, 2017, **358**, 745–750.
2 X. He, Y. Qiu and S. Yang, *Adv. Mater.*, 2017, **29**, 1700775.
3 L. N. Quan, B. P. Rand, R. H. Friend, S. G. Mhaisalkar, T.-W. Lee and E. H. Sargent, *Chem. Rev.*, 2019, **119**, 7444–7477.
4 L. Protesescu, S. Yakunin, M. I. Bodnarchuk, F. Krieg, R. Caputo, C. H. Hendon, R. X. Yang, A. Walsh and M. V. Kovalenko, *Nano Lett.*, 2015, **15**, 3692–3696.
5 Q. Zhang and Y. Yin, *ACS Cent. Sci.*, 2018, **4**, 668–679.
6 Q. A. Akkerman, G. Rainò, M. V. Kovalenko and L. Manna, *Nat. Mater.*, 2018, **17**, 394–405.
7 J. Shamsi, A. S. Urban, M. Imran, L. De Trizio and L. Manna, *Chem. Rev.*, 2019, **119**, 3296–3348.
8 J. Song, J. Li, X. Li, L. Xu, Y. Dong and H. Zeng, *Adv. Mater.*, 2015, **27**, 7162–7167.
9 T. Chiba, Y. Hayashi, H. Ebe, K. Hoshi, J. Sato, S. Sato, Y.-J. Pu, S. Ohisa and J. Kido, *Nat. Photonics*, 2018, **12**, 681–687.
10 S. Hou, M. K. Gangishetty, Q. Quan and D. N. Congreve, *Joule*, 2018, **2**, 2421–2433.
11 Y. Dong, Y.-K. Wang, F. Yuan, A. Johnston, Y. Liu, D. Ma, M.-J. Choi, B. Chen, M. Chekini, S.-W. Baek, L. K. Sagar, J. Fan, Y. Hou, M. Wu, S. Lee, B. Sun, S. Hoogland, R. Quintero-Bermudez, H. Ebe, P. Todorovic, F. Dinic, P. Li, H. T. Kung, M. I. Saidaminov, E. Kumacheva, E. Spiecker, L.-S. Liao, O. Voznyy, Z.-H. Lu and E. H. Sargent, *Nat. Nanotechnol.*, 2020, **15**, 668–674.
12 H. Chen, L. Fan, R. Zhang, C. Bao, H. Zhao, W. Xiang, W. Liu, G. Niu, R. Guo, L. Zhang and L. Wang, *Adv. Opt. Mater.*, 2020, **8**, 1901390.
13 L. Xu, J. Li, B. Cai, J. Song, F. Zhang, T. Fang and H. Zeng, *Nat. Commun.*, 2020, **11**, 3902.
14 Y.-H. Kim, S. Kim, A. Kakekhani, J. Park, J. Park, Y.-H. Lee, H. Xu, S. Nagane, R. B. Wexler, D.-H. Kim, S. H. Jo, L. Martínez-Sarti, P. Tan, A. Sadhanala, G.-S. Park, Y.-W. Kim, B. Hu, H. J. Bolink, S. Yoo, R. H. Friend, A. M. Rappe and T.-W. Lee, *Nat. Photonics*, 2021, **15**, 148–155.
15 T. Fang, T. Wang, X. Li, Y. Dong, S. Bai and J. Song, *Sci. Bull.*, 2021, **66**, 36–43.
16 G. Li, F. W. R. Rivarola, N. J. L. K. Davis, S. Bai, T. C. Jellicoe, F. de la Peña, S. Hou, C. Ducati, F. Gao, R. H. Friend, N. C. Greenham and Z.-K. Tan, *Adv. Mater.*, 2016, **28**, 3528–3534.
17 Y. Wei, X. Li, Y. Chen, Z. Cheng, H. Xiao, X. Li, J. Ding and J. Lin, *J. Phys. Chem. Lett.*, 2020, **11**, 1154–1161.
18 J. De Roo, M. Ibáñez, P. Geiregat, G. Nedelcu, W. Walravens, J. Maes, J. C. Martins, I. Van Driessche, M. V. Kovalenko and Z. Hens, *ACS Nano*, 2016, **10**, 2071–2081.
19 C. Zhang, B. Wang, W. Zheng, S. Huang, L. Kong, Z. Li, G. He and L. Li, *Nano Energy*, 2018, **51**, 358–365.
20 K. Yang, F. Li, Y. Liu, Z. Xu, Q. Li, K. Sun, L. Qiu, Q. Zeng, Z. Chen, W. Chen, W. Lin, H. Hu and T. Guo, *ACS Appl. Mater. Interfaces*, 2018, **10**, 27374–27380.
21 J. Song, J. Li, L. Xu, J. Li, F. Zhang, B. Han, Q. Shan and H. Zeng, *Adv. Mater.*, 2018, **30**, 1800764.
22 J. Song, T. Fang, J. Li, L. Xu, F. Zhang, B. Han, Q. Shan and H. Zeng, *Adv. Mater.*, 2018, **30**, 1805409.
23 F. Di Stasio, I. Ramiro, Y. Bi, S. Christodoulou, A. Stavrinadis and G. Konstantatos, *Chem. Mater.*, 2018, **30**, 6231–6235.
24 Z. Shi, S. Li, Y. Li, H. Ji, X. Li, D. Wu, T. Xu, Y. Chen, Y. Tian, Y. Zhang, C. Shan and G. Du, *ACS Nano*, 2018, **12**, 1462–1472.
25 P. Wang, Z. Wu, M. Wu, J. Wei, Y. Sun and Z. Zhao, *J. Mater. Sci.*, 2021, **56**, 4161–4171.
26 C. K. Trinh, H. Lee, M. G. So and C.-L. Lee, *ACS Appl. Mater. Interfaces*, 2021, **13**, 29798–29808.
27 B. Chen, L. Zhao, J. Ding, L. Wang, X. Jing and F. Wang, *Chem. Commun.*, 2016, **52**, 12052–12055.
28 Z. Zhong, X. Wang, T. Guo, J. Cui, L. Ying, J. Peng and Y. Cao, *Org. Electron.*, 2018, **53**, 35–42.